Electron tomography of early melanosomes: Implications for melanogenesis and the generation of fibrillar amyloid sheets

Ilse Hurbain[a,b], Willie J. C. Geerts[c], Thomas Boudier[d], Sergio Marco[e,f], Arie J. Verkleij[c], Michael S. Marks[g], and Graça Raposo[a,b,1]

[a]Institut Curie, Centre de Recherche, and [b]Unité Mixte de Recherche 144, Centre National de la Recherche Scientifique, F-75248 Paris, France; [c]Department of Cellular Architecture and Dynamics, Universiteit Utrecht, Padualaan 8, 3584 CH, Utrecht, The Netherlands; [d]Centre National de la Recherche Scientifique Université Pierre et Marie Curie, Unité Mixte de Recherche 7101, 75252 Paris Cedex 05, France; [e]Institut Curie, Centre de Recherche, F-91405 Orsay, France; [f]Institut National de la Santé et de la Recherche Médicale, Unité Mixte de Recherche 759, F-91405 Orsay, France; and [g]Department of Pathology and Laboratory Medicine, University of Pennsylvania, Philadelphia, PA, 19104-6100

Edited by David D. Sabatini, New York University School of Medicine, New York, NY, and approved August 27, 2008 (received for review April 15, 2008)

Melanosomes are lysosome-related organelles (LROs) in which melanins are synthesized and stored. Early stage melanosomes are characterized morphologically by intralumenal fibrils upon which melanins are deposited in later stages. The integral membrane protein Pmel17 is a component of the fibrils, can nucleate fibril formation in the absence of other pigment cell-specific proteins, and forms amyloid-like fibrils in vitro. Before fibril formation Pmel17 traffics through multivesicular endosomal compartments, but how these compartments participate in downstream events leading to fibril formation is not fully known. By using high-pressure freezing of MNT-1 melanoma cells and freeze substitution to optimize ultrastructural preservation followed by double tilt 3D electron tomography, we show that the amyloid-like fibrils begin to form in multivesicular compartments, where they radiate from the luminal side of intralumenal membrane vesicles. The fibrils in fully formed stage II premelanosomes organize into sheet-like arrays and exclude the remaining intralumenal vesicles, which are smaller and often in continuity with the limiting membrane. These observations indicate that premelanosome fibrils form in association with intralumenal endosomal membranes. We suggest that similar processes regulate amyloid formation in pathological models.

amyloid fibrils | premelanosomes | multivesicular bodies | Pmel17

Melanins are synthesized by skin and eye pigment cells within lysosome-related organelles called melanosomes. Melanosomes form through a series of morphologically defined stages, such that mature electron dense stage IV melanosomes with tightly packed melanins develop from specialized nonpigmented immature stage I and II melanosomes and partially pigmented stage III melanosomes (1); each stage represents a distinct biogenetic intermediate (see ref. 2; reviewed in ref. 3). Ellipsoidal shaped stage II and III organelles harbor characteristic intralumenal striations, or fibrils, organized in linear arrays through the length of the organelle. In highly pigmented cells, the fibrils in the majority of melanosomes are covered with melanin deposits (stage III), indicating that the fibrils serve to focus melanin polymerization within melanosomes. The fibrils are also thought to sequester highly reactive melanin intermediates, thus reducing the toxicity associated with melanin synthesis (4–6). Accordingly, animals in which melanosome fibrils do not form properly often become hypopigmented, likely because of melanocyte death (reviewed in ref. 7). Moreover, the melanosome fibrils resemble amyloids that form under pathological situations such as Alzheimer's disease and the prion encephalopathies (8–10). It is therefore important to understand how the fibrils form and organize to gain insight into neurodegenerative disorders.

The membrane trafficking events required for the generation of stage I and II premelanosomes and their intralumenal fibrils are poorly understood (reviewed in ref. 3). The premelanosome fibrils appear to be composed largely of luminal fragments of Pmel17/gp100, a pigment-cell-specific integral membrane protein (11–14). Expression of Pmel17 alone in nonmelanocytic HeLa cells induces the formation of similar fibrils within late endosomes (11), and a recombinant luminal Pmel17 Mα fragment forms amyloid-like fibrils upon renaturation in vitro (6). Pmel17 luminal fragments are enriched in stage II melanosomes but not easily detected in stage III and IV melanosomes (2), most likely because of encapsulation by melanin and masking of epitopes (3, 15).

Full-length Pmel17 can also be detected in endosomal compartments that correspond to stage I premelanosomes (2). These vacuolar compartments, which typically harbor a few detectable intralumenal vesicles (ILVs), contain Pmel17 both at their limiting membrane and on the ILVs, are accessed by endocytic tracers after 15 min, and bear at their cytosolic side bilayered coats containing clathrin (2) and the endosomal sorting complex required for transport (ESCRT)-0 component Hrs (16). These compartments are both morphologically and compositionally indistinguishable from bona fide endosomal vacuoles that function in nonmelanocytic cell types as intermediates in the down-regulation of membrane proteins, including the epidermal growth factor and growth hormone receptors, by the ESCRT-dependent multivesicular body (MVB) pathway (17, 18). We and others have defined such compartments as "coated endosomes" (2) or early MVBs (19). Pmel17, like growth factor receptors, is sequestered on the ILVs of early MVBs but paradoxically in a manner that is independent of ubiquitination, Hrs, and components of the ESCRT-I machinery (16). Pmel17 sequestration on ILVs precedes its proteolytic processing by a prohormone convertase to liberate the amyloidogenic luminal Mα fragment (12, 16) and is therefore essential for the generation of the amyloid-like fibrils of stage II premelanosomes. Whether the ILVs subserve additional functions in Pmel17 fibril formation is not yet known.

The structural events that follow Pmel17 cleavage to generate first morphologically detectable fibrils and then organized fibrillar arrays are not understood. Here, we use high-pressure freezing (HPF) and electron tomography (ET) to define at high resolution the internal organization of early melanosomal intermediates and

Author contributions: I.H., W.J.C.G., M.S.M., and G.R. designed research; I.H. and W.J.C.G. performed research; I.H., W.J.C.G., T.B., S.M., A.J.V., and G.R. analyzed data; and M.S.M. and G.R. wrote the paper.

The authors declare no conflict of interest.

This article is a PNAS Direct Submission.

[1]To whom correspondence should be addressed at: Institut Curie, Unité Mixte de Recherche 144, Centre National de la Recherche Scientifique, 26 Rue d'Ulm, 75248 Paris Cedex, France. Email: graposo@curie.fr.

This article contains supporting information online at www.pnas.org/cgi/content/full/0803488105/DCSupplemental.

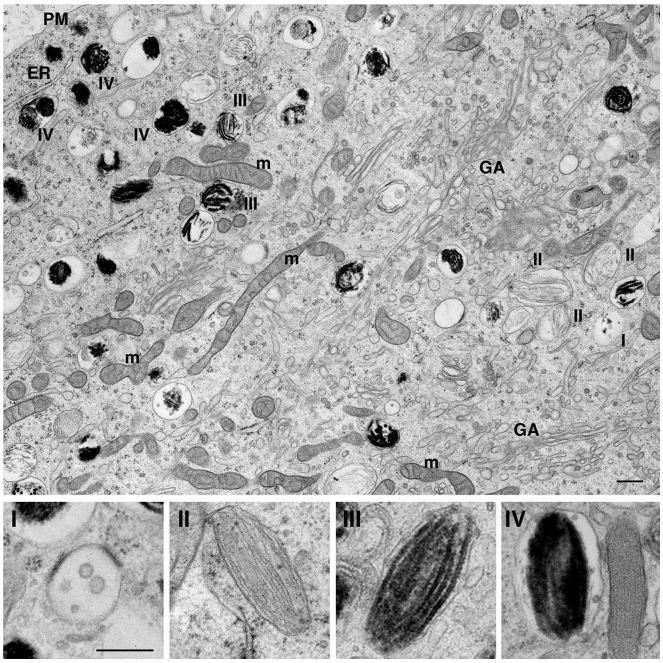

Fig. 1. Ultrastructure of MNT-1 cells using HPF and freeze substitution. (*Upper*) A low-magnification image showing mature melanosomes (stages IV and III) at the periphery and immature melanosomes (stages II and I) in the Golgi area. PM, plasma membrane; GA, Golgi Apparatus; m, mitochondria; ER, endoplasmic reticulum. (*Lower*) Selected images of stage I, II, III, and IV melanosomes. (Scale bars: 200 nm.)

of unpigmented stage II premelanosomes. The results elucidate an unexpectedly higher organization of the fibrils, suggest a direct role for ILVs in the early steps of fibril generation, and reveal a direct link between early MVBs, the generation of amyloid-like fibrils, and biogenesis of stage II premelanosomes.

Results

Preservation of Melanocyte Ultrastructure by HPF. MNT-1, a pigmented melanoma cell line, is an excellent model system to investigate the biogenesis of melanosomes (2, 11, 12, 20). MNT-1 cells resemble untransformed skin melanocytes by expression of mRNAs encoding melanogenic proteins (21) and by ultrastructure, in that melanosomes of all four stages (1) are detected by EM analysis after chemical fixation and embedding in epon resins (2). To better visualize intermediates in melanosome biogenesis, we have used HPF and freeze substitution. In HPF, cells are cryoimmobilized under high pressure in milliseconds, thus preserving their cytoplasm and organelles in a more natural state and bypassing potential artifacts caused by slow aldehyde fixation (22, 23). Cells are subsequently embedded in epon resin during freeze substitution (23). As shown in Fig. 1, the cytoplasm of MNT-1 cells preserved by this method is filled with distinct melanosomal structures, an extended Golgi apparatus, and numerous mitochondria. Pigmented, mature melanosomes (stages III and IV) are most abundant at the cell periphery, whereas unpigmented, immature melanosomes (stages I and II) are more concentrated in the Golgi area. The morphology of melanosomes in this analysis is seemingly similar to that obtained with glutaraldehyde fixation (1, 2), except that most organelles are slightly increased in volume, as previously described for other organelles, because HPF prevents aldehyde-induced shrinkage (24, 25). Notably, the organized arrays of intralumenal fibrils within immature melanosomes are well preserved.

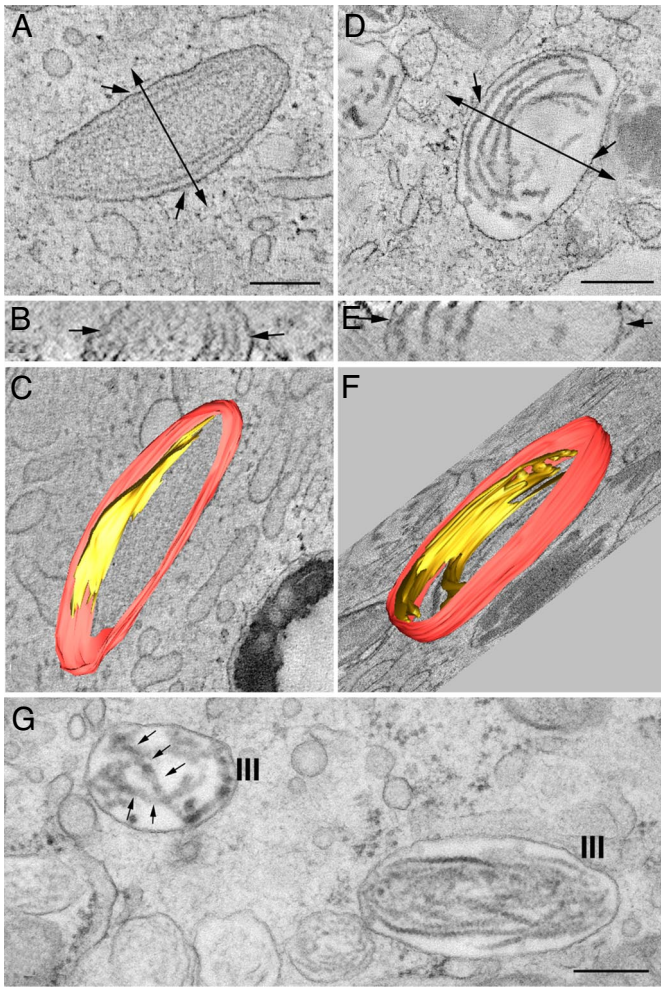

Fig. 2. The intralumenal fibrils of stage II premelanosomes are organized as sheets. (*A*) Slice of an electron tomographic reconstruction of a stage II premelanosome. The line indicates the axis of rotation for visualization along the *z* axis in *B*. (*A* and *B*) The intralumenal striations follow the curvature of the melanosomal membrane (arrows), revealing a sheet-like morphology. (*C*) Three-dimensional model of the melanosomal membrane (in magenta) and one single fibril (in yellow) (see Movie S1). (*D*) Slice of a reconstruction of a stage III melanosome. The line indicates the axis of rotation for visualization along the *z* axis in *E*. (*D* and *E*) Note the melanin deposits over the sheets. (*F*) Three-dimensional model of the melanosomal membrane (in magenta) and one single fibril with melanin (in yellow) (see Movie S2). (*G*, *Left*) A cross section through an early stage III melanosome reveals the sheet-like organization of the melanin-coated fibrillar structures (*Left*, arrows) as compared to the elongated fibrillar appearance of the longitudinally sectioned melanosome (*Right*). (Scale bars: 200 nm.)

Premelanosome Amyloid Fibrils on Which Melanin Deposits Are Organized as Sheets. The improved preservation by HPF allowed us to investigate in detail the ultrastructural characteristics of melanosome precursors in situ. We first sought to better define the nature of the organized fibrils within stage II melanosomes. To appreciate these structures in 3D, we performed double tilt tomographic reconstruction of thick (350–400 nm) sections of MNT-1 cells. Perpendicular tilt series were recorded in regions of the MNT-1 cell cytoplasm containing unpigmented stage II melanosomes, and tomographic slices were obtained [supporting information (SI) Movie S1]. In several reconstructions of nonpigmented stage II melanosomes (illustrated in the single slice shown in Fig. 2*A*), the intralumenal fibrils were measured to be 6–10 nm in diameter, similar to pathological amyloid fibrils (26) and fibrils generated by recombinant Pmel17 (6). Analysis of tomographic reconstructions

CELL BIOLOGY

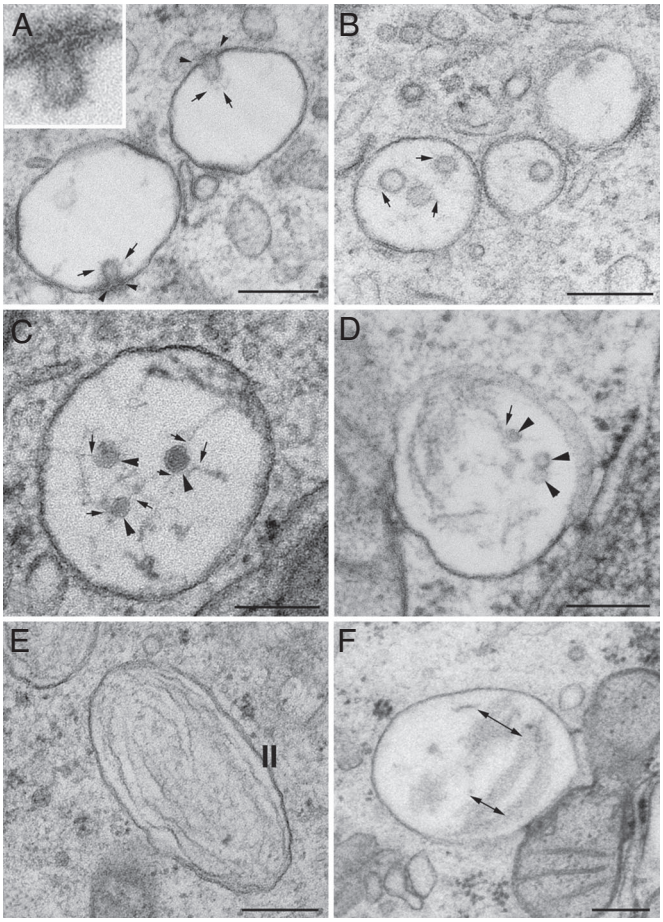

Fig. 3. Fibrils begin to form on ILVs within early MVBs. Small fibrils (arrows) are closely associated to nascent buds (*A*, see *Inset* for higher magnification) and vesicles of early MVBs (*B*, *C*, and *D*). (*B*) Examples of MVBs in which thin fibrils are seen emanating from 60–70 nm intralumenal vesicles (arrows). (*C* and *D*) Examples of organelles bearing smaller, 40-nm vesicles (arrowheads) and more organized fibrils (arrows). (*E*) An example of an ellipsoidal stage II premelanosome with organized arrays of fibrils (II). (*F*) Note the sheet-like appearance of the fibrils lying parallel to the plane of the section (double arrows). (Scale bars: 200 nm.)

on the *x–z* plane perpendicular to the fibrils (Fig. 2*B*; arrow in *A* indicates the axis of rotation) reveals that fibrils that appear to be separated in the x-y plane are actually continuous in the *x–z* plane (Fig. 2*B*). A partial 3D model obtained from manual contouring on tomographic slices (see *Materials and Methods*), highlighting the melanosomal membrane and a single fibril (Fig. 2*C* and Movie S1), reveals that the parallel fibrils are organized as sheets rather than separable "tubules." Similar analyses of fibrils with melanin deposits in a stage III melanosome reveal that melanin deposition increases the thickness of the fibrils 2-fold to a diameter of 14–20 nm (Fig. 2*D*; tomographic reconstruction in Movie S2). The melanin deposits are observed over the entirety of the organized fibrils, which retain their sheet-like organization as observed by tilting the reconstruction along its *z* axis (Fig. 2*E*) and by 3D modeling (Fig. 2*F* and Movie S2). In ultrathin sections of HPF-fixed MNT-1 cells, the sheets can be appreciated in slightly pigmented stage III melanosomes cut perpendicular to the plane of the section (Fig. 2*G*, arrows) relative to stage II melanosomes cut parallel to the plane of the section (Fig. 3*F* and Fig. S1*B*). Together, these results indicate that the Pmel17-containing fibrils of melanosome precursors assemble into 3D sheets like other amyloids and do not exist as isolated tubules like the microtubules in flagella (27) or the von Willebrand factor (vWF) polymers in Weibel–Palade bodies (WPBs) (28).

HPF Reveals Early Intermediates in Premelanosome Biogenesis. We next sought to better define the stage-I-like compartments in which amyloid-like fibrils begin to form. Compared to nonpigmented cells, MNT-1 cells display unusually numerous early MVBs/stage I melanosomes bearing coats on the limiting membrane (Fig. 1), inward budding profiles (Fig. 3*A*), and 1–4 internal vesicles with a diameter of 50–90 nm (Fig. 3*B*). Preservation by HPF reveals that in many of these "early stage I" compartments, very short and thin fibrillar structures (1.3–2.4 nm in diameter), are closely apposed to the inward invaginations and the ILVs and often appear to emanate from them (arrows in Fig. 3 *A* and *B*). In most cases, fibrils emanate from several distinct sites of individual ILVs, suggesting that the ILVs may seed the formation of multiple fibrils. Longer, thicker fibrils (6–8 nm in diameter) are observed in more ellipsoidal membrane-bound compartments (late stage I) displaying smaller ILVs (mean diameter of 30–45 nm) that appear more electron dense than those that are observed in early stage I (Fig. 3 *C* and *D* and Fig. S1*A*). These late stage I compartments, like fully formed, ellipsoidal stage II premelanosomes (Fig. 3*E* and Fig. S1*A*), are enriched in the perinuclear area and segregated from most mature melanosomes in the cell periphery. The size of the ILVs within early and late stage I melanosomes is generally inversely correlated with the size and amount of organized fibrils; early stage I harbor thin, short fibrils adjacent to larger vesicles, whereas late stage I harbor thicker, longer, and more organized fibrils with smaller vesicles (Table S1). These observations suggest that the late stage I structures are intermediates in the transition from early stage I to mature stage II premelanosomes and that fibril maturation is accompanied by a decrease in ILV size.

Pmel17-Driven Amyloid-Like Fibrils Are Closely Associated with the ILVs. The data in Fig. 3, in context with earlier findings (12, 16), suggest that fibrils generated upon Pmel17 cleavage directly emanate from inward budding profiles and ILVs. To further test for the association between the ILVs and nascent fibrils in 3D, we analyzed thick (350–400 nm) sections of MNT-1 cells by electron tomography. Double tilt series were recorded in regions enriched for early and late stage I melanosomes and processed for tomographic reconstruction (Movie S3*A*). Tomographic slices (with or without manual contours) of a single representative compartment containing both ILVs and fibrils are shown in Fig. 4 *A–C* and Movie S3*A*. Apparent within this organelle (Fig. 4*D* and Movie S3*B*) and others like it are several "free" ILVs, ranging in diameter from 25 to 50 nm, that are in this example not continuous with the limiting membrane. Fibrils emanate from most of the ILVs but are preferentially associated with the larger (50 nm) vesicles (Fig. 4*E*, for highlight at a different angle of the 3D model and Movie S3*A* and Movie S3*B*). In Fig. 4*F* and Movie S3*C*, a computational approach [the isosurface selection tool in the image processing, modelling and display (IMOD) program; see *Materials and Methods*] depicts fibrillar structures emanating from the larger ILVs, confirming the manual contouring in Fig. 4 *C–E*. These data suggest that the ILVs seed the formation of multiple individual fibrils.

The progressive fibril accumulation and reduction in ILV size within melanosome precursor compartments correlates with a transition from a round to an ellipsoid shape (see Fig. 3 *C* and *D*, Fig. S1*A*, and Table S1), such that early stage I structures are more rounded (Fig. 3*B*) and late stage I structures are more elongated (see also Fig. S1*A*). These data indicate that the accumulation of fibrils and decrease in number and diameter of ILVs are accompanied by the deformation of the limiting membrane as a first step toward acquiring the characteristic ellipsoidal shape of stage II premelanosomes.

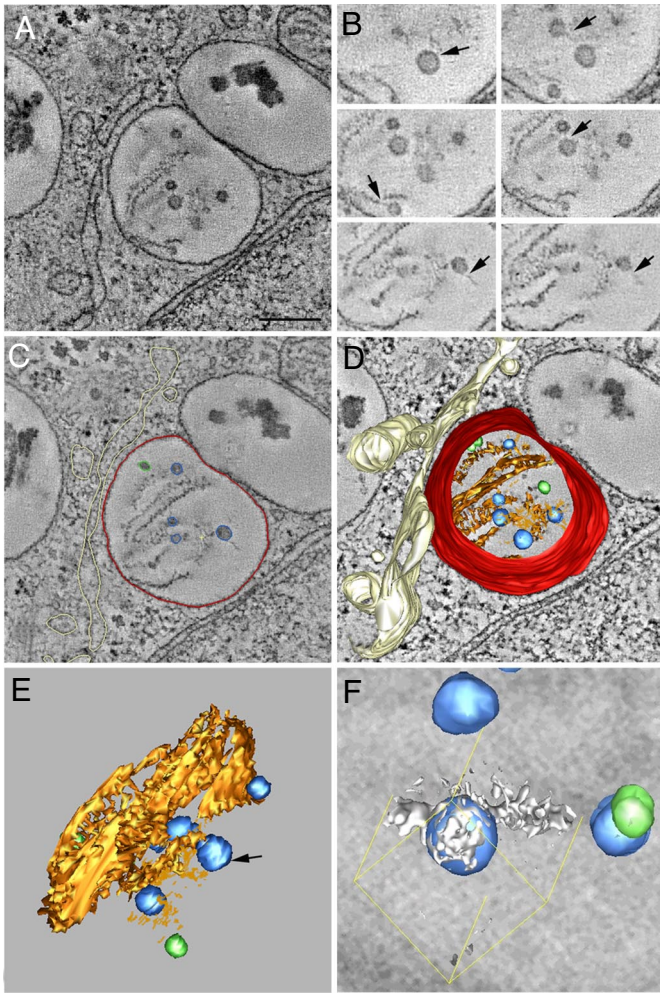

Fig. 4. Fibrils are closely associated with ILVs of early MVBs. (*A* and *B*) A tomogram slice (*A*) and sequential *z* axis slices through the tomographic volume (*B*) showing close association of small fibrils (arrows) with intralumenal vesicles. (*C* and *D*) Membranes and fibrils in consecutive tomogram slices are manually contoured; one slice is shown in *C*, and the 3D model is shown in *D*. The limiting membrane of the organelle is in red, vesicles with clearly associated fibrils (yellow) are in blue and those with no obvious fibrils are in green. Closely apposed endoplasmic reticulum membranes are in white. (*E*) The ILVs and associated fibrils are highlighted and shown rotated. Note the short fibrils emanating from larger ILVs. Arrow indicates the vesicle shown in *F*. (*F*) Computationally detected fibrils emanating from a large ILV. See also Movie S3*A* for tilt series and tomographic reconstruction, Movie S3*B* for 3D model, and Movie S3C for representation of fibrils by isosurfacing. (Scale bar: 200 nm.)

Stage II Premelanosomes Contain ILVs Continuous with the Limiting Membrane. In ultrathin sections of aldehyde-fixed MNT-1 cells or other melanocytic cells, ILVs are rarely observed within stage II premelanosomes bearing organized fibrillar sheets. This lack of detection likely reflects extraction of ILVs during preparation of sections, because small ILVs are observed within stage II melanosomes in thin sections (Fig. S1*C*) or tomographic reconstructions of thick sections (Fig. 5 and Movie S4*A*) of HPF-fixed MNT-1 cells. These ILVs range in size from 25 to 40 nm, similar to those observed in late stage I compartments (see Figs. 3 and 4 and Fig. S1). Importantly, however, they are segregated from the fibrillar sheets and accumulate preferentially between the organized fibrillar arrays and the limiting membrane (Fig. S1*C*), much like the ILVs within fibril-containing late MVBs of HeLa cells that ectopically express Pmel17 (11, 12). Most ILVs are detected in close proximity to, and often in continuity with, the limiting membrane of the stage

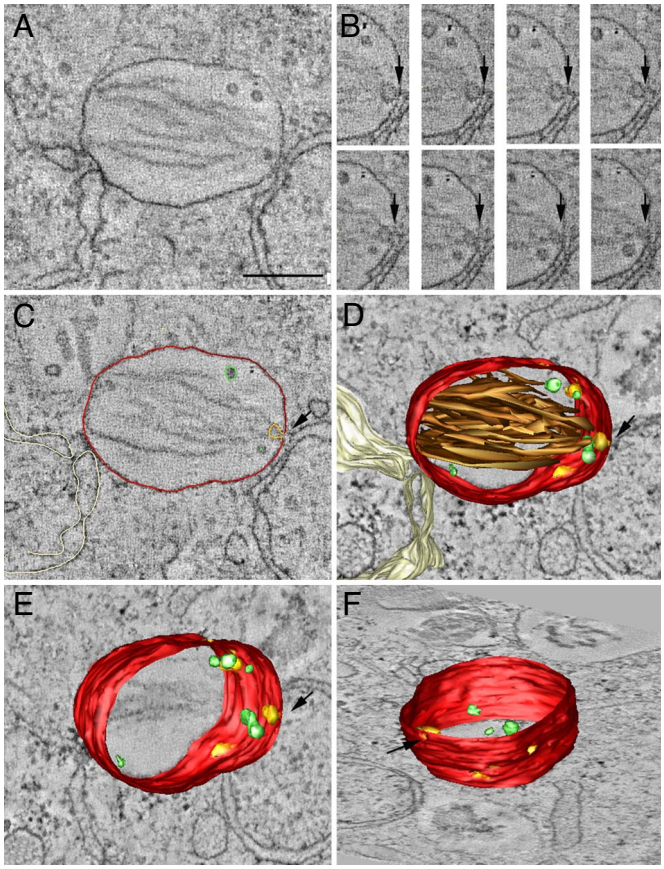

Fig. 5. Stage II premelanosomes bear ILVs continuous with the limiting membrane. (*A* and *B*) A tomogram slice (*A*) and sequential *z* axis slices through the tomographic volume (*B*) illustrating an internal vesicle fused with the limiting membrane of a stage II melanosome. (*C* and *D*) Membranes and fibrils in consecutive slices from the tomogram are manually contoured; one slice is shown in *C*, and the 3D model is shown in *D*. The limiting membrane of the organelle is in red; free vesicles are in green and those fusing with the membrane in yellow. Fibrils are in brown. Closely apposed endoplasmic reticulum membranes are in white. (*E* and *F*) The melanosomal membrane and the ILVs are highlighted. Note the continuities between the ILVs (yellow) and the melanosomal membrane, indicated by the appearance of the ILV membrane on the cytosolic face of the melanosome (arrows). See also Movie S4*A* for tilt series and tomographic reconstruction, Movie S4*B* for manual contouring, and Movie S4C for 3D model. (Scale bar: 200 nm.)

II premelanosomes. For example, in the representative 3D reconstruction in Fig. 5 *E* and *F* (Movie S4*B* and Movie S4*C*), the membrane of three out of eight ILVs is continuous with the organelle limiting membrane (see also Fig. S2). These observations suggest that, once the fibrils organize in parallel arrays, the remaining ILVs may be forced to the periphery of the now ellipsoidal organelle. The observed continuities with the limiting membrane might represent "back fusion" of the remnants of fibril-associated ILVs, potentially explaining why stage II premelanosomes contain less ILVs. However, we cannot exclude that they might represent inward budding events from the limiting membrane to generate new "free" vesicles bearing later stage melanosome cargoes, like tyrosinase (20) and ATP7A (29).

Discussion

Here we have used HPF and 3D double tilt electron tomographic analyses of MNT-1 melanocytic cells to define the ultrastructural organization of the intralumenal fibrillar matrix of melanosomes and the relationship between nascent fibrils and the ILVs of melanosome precursors. Our observations shed light on a critical

step of melanogenesis and open an avenue for understanding how pathological amyloid fibers are formed and regulated.

Our detailed characterization of fibrils and ILVs in melanosome precursors was made possible by HPF and freeze substitution, which preserves cellular architecture to a degree unobtainable with chemical fixation. HPF preserved ILVs and associated small protofibrils within intermediates in the formation of stage II melanosomes; such structures are likely altered or destroyed by the chemical fixation and subsequent organic extraction used in conventional EM analyses. HPF has been similarly exploited to advance our understanding of the early steps of WPB biogenesis in human umbilical vein endothelial cells, allowing Zenner and coworkers to observe vWF-containing tubules in the *trans* Golgi network and associated vesicular structures (28). Whereas single tilt tomograms have been useful in defining subcellular structures in 3D (30), we used double tilt 3D electron tomography—combining two perpendicular tilt series—to reduce the so-called "missing wedge" into a "missing cone" (31, 32) and thereby improve resolution along the z axis. In single tilt series of $\pm$ 60°, only 67% of Fourier space is covered resulting in elongation of structures parallel to the optical axis. By combining 2 perpendicular tomograms in a single double tilt reconstruction, 84% of Fourier space is covered resulting in a more isoform resolution of the final tomogram and less distortions along the z axis (33). The 3D resolution afforded by combining HPF with double tilt electron tomography allowed us to reveal aspects of intermediates in stage II melanosome formation, similar to the advances provided by 3D analyses in understanding the organization of forming WPBs (34), MVBs (25) and multilamellar MHC class II compartments (35).

Our 3D analyses of stage II premelanosomes show that fully matured fibrils are organized as parallel sheets rather than as separable fibrils. This sheet-like arrangement is unique among intralumenal structures within subcellular organelles, and contrasts with the isolated tubules formed by vWF in WPBs (28). Thus, although fibril formation by both Pmel17 and vWF are initiated by an analogous proteolytic activation step (12, 36), the polymerized structures generated from their cleavage products are dramatically different. The tendency to aggregate fibrils into sheets or not must therefore be regulated either by inherent features of nonamyloidogenic regions of fibril components (i.e., Pmel17 and vWF) or by accessory factors. Interestingly, sheet-like organizations have been observed for other amyloidogenic proteins such as the Aβ peptide in Alzheimer's disease and thus might represent a characteristic of amyloid fibrils (37). Deposition of Pmel17 in sheets might provide a platform for melanin aggregation into a large contiguous structure. This sheet-like organization might facilitate transfer of polymerized melanins in a single package from epidermal melanocytes to keratinocytes or prevent release of polymerized melanins from melanosomes during transient fusion with phagosomes in retinal pigment epithelial cells.

We had previously shown that proteolytic processing of Pmel17 to the amyloidogenic Mα fragment requires sorting onto the ILVs of MVBs (11, 12, 16). Our analyses here reveal an intimate relationship between ILVs and newly forming fibrils and add to the increasing evidence supporting a role for MVBs and their ILVs and exosomes (secreted forms of ILVs) in the formation of pathogenic amyloid fibrils (38–40). MVBs may provide an environment conducive for the proteolytic processing and unfolding of amyloidogenic precursors by virtue of a mildly acidic pH and a balanced cohort of processing proteases (41–43). In addition, the unique cohort of "raft-like" lipids associated with ILVs—particularly cholesterol, ceramide, and glycosphingolipids (44–47)—might facilitate amyloidogenesis (48, 49). Consistent with this notion, raft-like structures are required for the processing of Alzheimer's precursor protein to the amyloidogenic Aβ peptide (50) and for the conformational changes that lead to the generation of the scrapie prion protein (51, 52); amyloid formation in monocytes can be impaired by cholesterol reduction (53); extracellular amyloid fibril formation can be induced by GM1 gangliosides associated with exosomes (40); and raft lipids are components of extracellular amyloid fibrils (53). Raft lipids might be recruited onto the forming fibrils directly from the ILVs, a hypothesis supported by the decrease in the number and diameter of the ILVs as the premelanosome fibrils grow and accumulate. Although raft lipids are not required for the rapid fibrillogenesis of recombinant Pmel17-Mα fragments diluted out of denaturant in vitro (6), they may be required to facilitate the conformational changes required for amyloidogenesis from folded forms of Pmel17 in vivo.

Our analyses of stage II melanosome development showed a correlation between elongation of fibrils and development of the characteristic ellipsoid shape of melanosomes. The growing sheet-like Pmel17 fibrillar matrix might act like an inner skeleton, generating a force that induces membrane deformation around the sheets. Similar deformation of lipid vesicles in vitro by confined, polymerizing microtubules has been shown to generate ellipsoid-like structures with a melanosome-like shape (54). This evidence might then explain how melanosomes of later stages maintain their shape and size.

Our analyses also revealed that, concomitant with elongation and organization of the fibrils, the small remaining ILVs within stage II melanosomes accumulate in the periphery of the organelles, some of them continuous with the limiting membrane. These continuities might represent inward budding of newly forming vesicles or back fusion of preexisting vesicles with the limiting membrane, as proposed to occur in dendritic cells as a mechanism by which MHC class II molecules on ILVs are reinserted into the limiting membrane of MVBs for ultimate exposure on the plasma membrane (55). Although speculative, we favor the hypothesis that the continuities that we observe represent back fusion for 2 reasons. First, maturation of premelanosomes is accompanied by a deformation of the precursor endosome as discussed above, and back fusion of ILVs that have released the amyloidogenic Pmel17 fragments could facilitate deformation and growth of the organelle by increasing the amount of limiting membrane. Second, whereas numerous ILVs are detected in stage I melanosomes, very few ILVs are detected in mature stage II premelanosomes; back fusion would provide a mechanism by which these ILVs would disappear. Back fusion would also provide a mechanism to remove unwanted components of the ILVs from the melanosome lumen, such as nonfibrillogenic Pmel17 Mβ fragments, and facilitate cytosolic exposure of effector molecules that are required for subsequent steps of melanosome maturation, such as fusion with transport intermediates carrying melanogenic enzymes. Consistently, our 3D tomographic analyses reveal close apposition—albeit not fusion—between premelanosomes and other organelles, including endosomal tubules (data not shown) and the ER (Fig. 4). Further studies are needed to determine the functional significance of these contacts and to resolve the vectoriality of fusion/budding events and the subsequent changes in limiting membrane composition that accompany premelanosome maturation.

Materials and Methods

HPF. MNT1 cells were cultured on carbonated sapphire discs (30 mm in diameter) for 4 days in DMEM containing 10% AIM V medium and 20% FCS as described (2). At 70% confluency they were high-pressure frozen with a EM PACT I (Leica Microsystems), the culture medium containing 20% of FCS serving as cryoprotectant (22).

Freeze Substitution. High-pressure frozen samples were transferred to the AFS (Leica Microsystems) with precooled substitution fluid (−90 °C) of anhydrous acetone, containing 2% osmium tetroxide. Substitution at −90 °C lasted for 45 h. Then the samples were warmed 2 °C per hour to −60 °C, where they remained for 12 h. The samples were warmed again with 2 °C per hour to −30 °C, where they remained for 8 h before being transferred to ice for 1 h. Thereafter, the substitution fluid was washed away by anhydrous acetone and the samples were embedded in Epon 812 (TAAB Laboratories Equipment). Polymerization was performed at 60 °C for 48 h.

Sample Preparation. Epon sections (350 nm thick) were cut on a Reichert Ultracut S microtome (Leica Microsystems) and collected on formvar-coated copper grids (75 mesh) for analysis by electron tomography. Sections were randomly labeled on the 2 sides with protein A-gold 10-nm and poststained with 2% uranylacetate in methanol for 4 min and lead citrate for 2 min.

Electron Tomography. Tilt series (2 perpendicular series per tomogram, angular range from −60° to + 60° with 1° increments) of 350-nm-thick sections were recorded automatically by using Xplore3D (FEI Company) on a 200-kV transmission electron microscope (Tecnai 20 LaB_6, FEI company) and used for reconstructing tomograms. Projection images (1024 × 1024 pixels) were recorded with a CCD camera (Temcam F214; TVIPS GmbH). After acquiring the first tilt series, the specimen grid was rotated over an angle of 90° and a second series was recorded of the same area. Alignment of the tilt series and tomogram computing (resolution-weighted back-projection) were carried out by using the IMOD program (32). The 10-nm gold particles at the surface of the sections were used as fiducial markers. Manual contouring of the tomograms was done by using the IMOD program (55). Finally, the contours were meshed and the *z* scale was stretched with a factor of 1.6 to correct for resin shrinkage (32). In addition to the manual contouring of fibrils, the isosurface selection tool in IMOD 3.12.10 allowed the computational identification of fibrillar structures emanating from the larger ILVs (55).

ACKNOWLEDGMENTS. We thank Daniel Studer (University of Bern, Bern, Switzerland) for advice with HPF; G. van Niel, C. Delevoye, M. Romao, D. Tenza, F. Giordano, and S. Simoes for discussions; and A. Roux, J.B. Manneville, and W. Stoorvogel for advice, comments, and preparation of the manuscript. This work was supported by Centre National de la Recherche Scientifique, Institut Curie, and Fondation pour la Recherche Médicale (to G.R.); Agence National de la Recherche Grant ANR-PCV06-142771 (to G.R. and S.M.); National Institutes of Health Grant R01 AR048155 (to M.S.M.); and 3DEM Network of Excellence (W.G. and A.V.).

1. Seiji M, Fitzpatrick TM, Simpson RT, Birbeck MSC (1963) Chemical composition and terminology of specialized organelles (melanosomes and melanin granules) in mammalian melanocytes. *Nature* 197:1082–1084.
2. Raposo G, Tenza D, Murphy DM, Berson JF, Marks MS (2001) Distinct protein sorting and localization to premelanosomes, melanosomes, and lysosomes in pigmented melanocytic cells. *J Cell Biol* 152:809–824.
3. Raposo G, Marks MS (2007) Melanosomes–dark organelles enlighten endosomal membrane transport. *Nat Rev Mol Cell Biol* 8:786–797.
4. Chakraborty AK, *et al*. (1996) Polymerization of 5,6-dihydroxyindole-2-carboxylic acid to melanin by the pmel 17/silver locus protein. *Eur J Biochem* 236:180–188.
5. Lee ZH, *et al*. (1996) Characterization and subcellular localization of human Pmel 17/*silver*, a 100-kDa (pre)melanosomal membrane protein associated with 5,6,-dihydroxyindole-2-carboxylic acid (DHICA) converting activity. *J Invest Dermatol* 106:605–610.
6. Fowler DM, *et al*. (2006) Functional amyloid formation within mammalian tissue. *PLoS Biol* 4:100–107.
7. Theos AC, Truschel ST, Raposo G, Marks MS (2005) The Silver locus product Pmel17/gp100/Silv/ME20: Controversial in name and in function. *Pigment Cell Res* 18:322–336.
8. Merlini G, Westermark P (2004) The systemic amyloidoses: Clearer understanding of the molecular mechanisms offers hope for more effective therapies. *J Internal Med* 255:159–178.
9. Chiti F, Dobson CM (2006) Protein misfolding, functional amyloid and human disease. *Annu Rev Biochem* 75:333–366.
10. Fowler DM, Koulov AV, Balch WE, Kelly JW (2007) Functional amyloid–from bacteria to humans. *Trends Biochem Sci* 32:217–223.
11. Berson JF, Harper D, Tenza D, Raposo G, Marks MS (2001) Pmel17 initiates premelanosome morphogenesis within multivesicular bodies. *Mol Biol Cell* 12:3451–3464.
12. Berson JF, *et al*. (2003) Proprotein convertase cleavage liberates a fibrillogenic fragment of a resident glycoprotein to initiate melanosome biogenesis. *J Cell Biol* 161:521–533.
13. Theos AC, *et al*. (2006) Dual loss of ER export and endocytic signals with altered melanosome morphology in the silver mutation of Pmel17. *Mol Biol Cell* 17:3598–3612.
14. Kushimoto T, *et al*. (2001) A model for melanosome biogenesis based on the purification and analysis of early melanosomes. *Proc Natl Acad Sci USA* 98:10698–10703.
15. Donatien PD, Orlow SJ (1995) Interaction of melanosomal proteins with melanin. *Eur J Biochem* 232:159–164.
16. Theos AC, *et al*. (2006) A lumenal domain-dependent pathway for sorting to intralumenal vesicles of multivesicular endosomes involved in organelle morphogenesis. *Dev Cell* 10:343–354.
17. Raiborg C, *et al*. (2002) Hrs sorts ubiquitinated proteins into clathrin-coated microdomains of early endosomes. *Nat Cell Biol* 4:394–398.
18. Sachse M, Urbe S, Oorschot V, Strous GJ, Klumperman J (2002) Bilayered clathrin coats on endosomal vacuoles are involved in protein sorting toward lysosomes. *Mol Biol Cell* 13:1313–1328.
19. Salas-Cortes L, *et al*. (2005) Myosin Ib modulates the morphology and the protein transport within multi-vesicular sorting endosomes. *J Cell Sci* 118:4823–4832.
20. Theos AC, *et al*. (2005) Functions of AP-3 and AP-1 in tyrosinase sorting from endosomes to melanosomes. *Mol Biol Cell* 16:5356–5372.
21. Hoek K, *et al*. (2004) Expression profiling reveals novel pathways in the transformation of melanocytes to melanomas. *Cancer Res* 64:5270–5282.
22. Studer D, Graber W, Al-Amoudi A, Eggli P (2001) A new approach for cryofixation by high pressure freezing. *J Microsc* 203:285–294.
23. Matsko N, Mueller M (2005) Epoxy resin as fixative during freeze substitution. *J Struct Biol* 152:92–103.
24. Murk JL, *et al*. (2003) Influence of aldehyde fixation on the morphology of endosomes and lysosomes: Quantitative analysis and electron tomography. *J Microsc* 212:81–90.
25. Murk JL, *et al*. (2003) Endosomal compartmentalization in three dimensions: Implications for membrane fusion. *Proc Natl Acad Sci USA* 100:13332–13337
26. Cohen AS, Calkins E (1959) Electron microscopic observations on a fibrous component in amyloid of diverse origins. *Nature* 183:1202–1203.
27. Song YH, Mandelkow E (1995) The anatomy of flagellar microtubules: Polarity, Seam, Junctions and Lattice. *J Cell Biol* 128:81–94.
28. Zenner HL, Collinson LM, Michaux G, Cutler DF (2007) High-pressure freezing provides insights into Weibel-Palade body biogenesis. *J Cell Sci* 120:2117–2125.
29. Setty SR, *et al*. (2008) Cell-specific ATP7A transport sustains copper-dependent tyrosinase activity in melanosomes. *Nature* 454:1142–1146.
30. Höög J, *et al*. (2007) Organization of interphase microtubules in fission yeast analyzed by electron tomography. *Dev Cell* 12:349–361.
31. Penczek P, Marko M, Buttle K, Frank J (1995) Double-tilt electron microscopy. *Ultramicroscopy* 60:393–410.
32. Mastronarde DN (1997) Dual-axis tomography: An approach with alignment methods that preserve resolution. *J Struct Biol* 120:343–352.
33. Kremer JR, Mastronarde DN, Mcintosh JR (1996) Computer visualization of three-dimensional image data using IMOD. *J Struct Biol* 116:71–76.
34. Valentijn KM, Valentijn JA, Jansen KA, Koster AJ (2008) A new look at Weibel-Palade body structure in endothelial cells using electron tomography. *J Struct Biol* 161:447–458.
35. Murk J, *et al*. (2004) 3-D Structure of multilaminar lysosomes in antigen presenting cells reveals trapping of MHC II on the internal membranes. *Traffic* 12:936–945.
36. Journet AM, Saffaripour S, Cramer EM, Tenza D, Wagner DD (1993) von Willebrand factor storage requires intact prosequence cleavage site. *Eur J Cell Biol* 60:31–41.
37. Dong J, Lu K, Lakdawala A, Mehta A, Lynn D (2006) Controlling amyloid growth in multiple dimensions. *Amyloid* 13:206–215.
38. Fevrier B, *et al*. (2004) Cells release prions in association with exosomes. *Proc Natl Acad Sci USA* 101:9683–9688.
39. Rajendran L, *et al*. (2006) Alzheimer's disease beta-amyloid peptides are released in association with exosomes. *Proc Natl Acad Sci USA* 103:11172–11177.
40. Yuyama K, Yamamoto N, Yanagisawa K (2007) Accelerated release of exosome-associated GM1 ganglioside (GM1) by endocytic pathway abnormality: Another putative pathway for GM1-induced amyloid fibril formation. *J Neurochem* 105:217–224.
41. Baron GS, Wehrly K, Dorward DW, Chesebro B, Caughey B (2002) Conversion of raft associated prion protein to the protease-resistant state requires insertion of PrP-res (PrP(Sc)) into contiguous membranes. *EMBO J* 21:1031–1040.
42. Pimpinelli F, Lehman S, Maridoneau-Parini I (2005) The scrapie prion protein is present in flotillin-1-positive vesicles in central- but not peripheral-derived neuronal cell lines. *Eur J Neurosc* 21:2063–2072.
43. Kovacs GG, *et al*. (2007) Involvement of the endosomal-lysosomal system correlates with regional pathology in Creutzfeldt-Jakob disease. *J Neuropathol Exp Neurol* 66:628–636.
44. Wubbolts R, *et al*. (2003) Proteomic and biochemical analyses of human B cell-derived exosomes. Potential implications for their function and multivesicular body formation. *J Biol Chem* 278:10963–10972.
45. Trajkovic K, *et al*. (2008) Ceramide triggers budding of exosome vesicles into multivesicular endosomes. *Science* 319:1244–1247.
46. Mobius W, *et al*. (2002) Immunoelectron microscopic localization of cholesterol using biotinylated and non-cytolytic perfringolysin O. *J Histochem Cytochem* 50:43–55.
47. Mobius W, *et al*. (2003) Recycling compartments and the internal vesicles of multivesicular bodies harbor most of the cholesterol found in the endocytic pathway. *Traffic* 4:222–231.
48. Chi EY, *et al*. (2008) Lipid membrane templates the ordering and induces the fibrillogenesis of Alzheimer's disease amyloid-beta peptide. *Proteins* 72:1–24.
49. Hartmann T, Kuchenbecker J, Grimm O (2007) Alzheimer's disease: The lipid connection. *J Neurochem* 103:159–170.
50. Ehehalt R, Keller P, Haass C, Thiele C, Simons K (2003) Amyloidogenic processing of the Alzheimer beta-amyloid precursor protein depends on lipid rafts. *J Cell Biol* 160:113–123.
51. Hooper NM (2005) Roles of proteolysis and lipid rafts in the processing of the amyloid precursor protein and prion protein. *Biochem Soc Trans* 33:335–338.
52. Pinheiro TJT (2006) The role of rafts in the fibrillization and aggregation of prions. *Chemand Physics of Lipids* 141:66–71.
53. Gellermann G, *et al*. (2005) Raft lipids as common components of human extracellular amyloid fibrils. *Proc Natl Acad Sci USA* 102:6297–6302.
54. Fygenson DK, Marko JF, Libchaber A (1997) Mechanics of microtubule-based membrane extension. *Phys Rev Lett* 79:4497–4500.
55. Kleijmeer M, *et al*. (2001) Reorganization of multivesicular bodies regulates MHC class II antigen presentation by dendritic cells. *J Cell Biol* 155:53–63.